Electron paramagnetic resonance study of hydrogen-vacancy defects in crystalline silicon

P. Stallinga, P. Johannesen,* S. Herstrøm, K. Bonde Nielsen, and B. Bech Nielsen
Institute of Physics and Astronomy, University of Aarhus, DK-8000 Aarhus C, Denmark

J. R. Byberg
Institute of Chemistry, University of Aarhus, DK-8000 Aarhus C, Denmark

(Received 6 February 1998)

Electron paramagnetic resonance measurements on float-zone silicon implanted with protons at ~50 K followed by heating to room temperature have revealed two signals $S1_a$ and $S1_b$ belonging to the $S1$ group of signals. $S1_a$ and $S1_b$ both originate from defects with spin $S=\frac{1}{2}$ and monoclinic-I symmetry. The near-trigonal g tensors and several sets of ^{29}Si hyperfine splittings all closely resemble those observed previously for $V\mathrm{H}^0$, the neutral charge state of the monovacancy binding a single hydrogen atom. Analysis of a tiny proton hyperfine splitting of $S1_a$ provides strong evidence that this signal originates from $V_2\mathrm{H}^0$, the neutral charge state of the divacancy binding one hydrogen atom. Parallel studies of the thermal decays of the $V\mathrm{H}^0$, $S1_a$, and $S1_b$ signals and of infrared-absorption lines associated with Si-H stretch modes indicate that $V\mathrm{H}^0$ possesses a stretch mode at 2038.5 cm^{-1}, whereas modes at 2068.1 and 2073.2 cm^{-1} originate from the $S1_a$ and $S1_b$ defects. On the basis of theoretical results, we argue that the 2068.1-cm^{-1} mode arises from $V_2\mathrm{H}^0$ (the $S1_a$ defect) whereas the 2073.2-cm^{-1} mode probably belongs to $V_n\mathrm{H}^0$, $n=3$ and 4 (the $S1_b$ defect).
[S0163-1829(98)05031-0]

I. INTRODUCTION

The properties of hydrogen impurities in crystalline silicon have been studied intensively in the past.[1,2] As a result of this effort, the structures of a number of hydrogen-related defects have been identified primarily by Fourier transform infrared (FTIR) spectroscopy,[3–6] Raman spectroscopy,[7,8] and ion channeling.[9,10] These techniques have given valuable information about local vibrational modes associated with hydrogen, and the numbers of hydrogen atoms as well as their positions within the defects have been determined. However, little direct information has in general been obtained about the electronic properties of hydrogen-related defects. Apart from the complexes formed when hydrogen combines with a group-III acceptor[3,9,10] or a group-V donor,[3,11] the isolated hydrogen atom at the bond-center site was until recently the only case in which both the structure of a hydrogen defect, i.e., the arrangement of atoms, and its electronic properties were convincingly established.[12–14]

In molecular compounds such as silane, hydrogen and silicon atoms form strong covalent bonds with a typical dissociation energy of ~3.3 eV, whereas only ~2.0 eV is required to break a Si-Si bond in crystalline silicon.[15] Therefore, we may expect that hydrogen atoms embedded in a silicon matrix will form Si-H bonds even when this implies the breaking of Si-Si bonds. In particular, the binding of hydrogen to vacancies is a strongly exoenergetic process because these defects possess weak, elongated Si-Si bonds as well as dangling bonds (silicon orbitals occupied by a single electron). Accordingly, vacancies should efficiently trap hydrogen atoms. This expectation was directly confirmed by a FTIR study[5] of proton-implanted silicon in which monovacancies binding two, three, and four hydrogen atoms were identified.

The neutral charge state of the monovacancy containing a single hydrogen atom $V\mathrm{H}^0$ was recently identified by electron paramagnetic resonance (EPR).[16] The EPR spectra revealed that $V\mathrm{H}^0$ has monoclinic-I symmetry (point-group C_{1h}), and that its electron-spin distribution corresponds to a single dangling bond attached to a silicon atom. In accordance with the expected strength of the Si-H bond, the electron spin density at the proton is negligible. The observed weak proton hyperfine interaction is fully accounted for in terms of the magnetic dipole-dipole interaction between the spins of the electron and the proton, considered as classical point dipoles ~2.7 Å apart.

In addition to becoming captured by monovacancies, hydrogen atoms may also become trapped at small vacancy clusters like the divacancy[17] V_2, the trivacancy[18] V_3, and the planar tetravacancy[18] V_4, all of which abound in silicon after implantation of protons. In the present work we discuss the neutral charge state of such clusters binding a single hydrogen atom each, which we denote collectively by $V_n\mathrm{H}^0$. Each member of this family of defects has an odd number of electrons and is therefore amenable to EPR study. It seems reasonable to assume that the electronic structures of $V_n\mathrm{H}^0$ resemble that of $V\mathrm{H}^0$. Hence, we may expect that the EPR signals from $V_n\mathrm{H}^0$ (like that from $V\mathrm{H}^0$) display the characteristics of a dangling bond in a vacancy-type defect. A major EPR signal, denoted $S1$, which answers this description, has previously been observed in proton-implanted silicon.[12,19–22] This signal so closely resembles the signal from $V\mathrm{H}^0$ that some care was required in our previous study to separate out the latter. $S1$ was in the past claimed to display either trigonal[19–21] or near-trigonal, monoclinic-I symmetry.[22] More recently, Gorelkinskii and Nevinnyi reported that $S1$ in fact consists of *two* signals in float-zone silicon displaying trigonal and monoclinic-I symmetries.[12] No microscopic models have been proposed for the defects giving rise to $S1$.

In the present investigation of proton- and deuteron-implanted float-zone silicon, we have identified two members of the $S1$ group of signals, which we label $S1_a$ and $S1_b$. Both signals originate from defects with monoclinic-I symmetry. The involvement of a single hydrogen atom in the underlying defects is demonstrated directly for $S1_a$, whereas it is inferred for $S1_b$. We argue that $S1_a$ originates from V_2H^0 and that $S1_b$ most likely originates from V_3H^0 and possibly also from V_4H^0. Parallel EPR and FTIR measurements on identical samples show that VH^0 possesses a Si-H stretch mode at 2038.5 cm^{-1}, and that two other Si-H stretch modes at 2068.1 and 2073.2 cm^{-1} are correlated with the $S1_a$ and $S1_b$ defects.

II. EXPERIMENTAL DETAILS

A. Sample preparation

Samples shaped as rectangular parallelepipeds measuring $15\times5\times0.5$ mm^3 with the large faces normal to the [111] axis and the small faces (5×0.5 mm^2) normal to the [110] axis were cut from float-zone silicon with a quoted content of carbon and oxygen below 10^{16} cm^{-3}. The material was uncompensated n type with a resistivity of ~600 Ω cm, corresponding to a phosphorus concentration of $\sim9\times10^{12}$ cm^{-3}. The samples were polished on both large faces, and were subsequently etched lightly in a mixture of HF and HNO_3 to remove surface defects.

During the implantation, the samples were mounted inside a vacuum chamber on a copper block, which was in good thermal contact with the cold finger of a closed-cycle helium cryocooler. The samples were cooled to a temperature of about 20 K, and implanted with protons or deuterons through 0.2-mm aluminum. The sample temperature rose as a result of the implantation, but was always kept below 130 K. The background pressure in the chamber was about 10^{-5} torr during the implantation. In the following, samples implanted with protons and deuterons are denoted Si:H and Si:D, respectively. Protons were implanted into one of the 15×5-mm^2 faces at 56 different energies in the range from 5.3 to 10.5 MeV, whereas deuterons were implanted into both 15×5-mm^2 faces at 38 different energies in the range from 5.0 to 10.6 MeV. The implantations were carried out in a sequence going from high to low energies. The dose at each energy was chosen to yield a nearly homogeneous concentration of hydrogen isotopes of about 3×10^{17} cm^{-3} throughout the sample. The ion beam was defocused and the lateral distribution was monitored with a beam scanner located between the sample and the slits defining the $\sim20\times7$-mm^2 beam spot. Thereby, the lateral distribution could be controlled and kept uniform to within $\sim20\%$ over the beam spot. At each energy, the flux of implants was determined before the implantation from the current measured in a calibrated beam cup with a 2-mm acceptance hole, and the implantation time was then calculated to yield the desired dose. The current typically fluctuated by $\sim20\%$, which gives a rough measure of the uncertainty of the implanted dose. After the implantation the samples were allowed to warm up to room temperature. At that point the samples were highly resistive due to compensation of the phosphorus donors throughout the sample. The implantation was carried out at low temperature rather than at room temperature because a previous FTIR study showed that low-temperature implantation reduces the number of different defect structures.

B. EPR measurements

EPR spectra were recorded with a Bruker ESP300E spectrometer operated in the absorption mode at ~9.2 GHz (X band), in conjunction with a Varian E-257 variable temperature device, which allowed the sample temperature to be set in the range 90–570 K by means of a thermostatted gas flow through a quartz dewar tube inserted into the microwave cavity. The sample was glued to a short brass rod, which was connected to a goniometer head by a stainless-steel capillary tube in order to minimize the thermal leak. The sample temperature was monitored with a copper-constantan thermocouple placed within the stainless-steel tube, in contact with the brass rod approximately 15 mm down stream from the sample.

The microwave frequency ν_0 and the static magnetic field $\mathbf{B}_0$ were monitored continuously during scans by means of a Hewlett-Packard 5350B frequency counter and a Bruker ER035M NMR gaussmeter. The NMR probehead was placed between the microwave cavity and one of the pole pieces of the magnet. The g factor measured for polycrystalline DPPH (diphenylpicrylhydrazyl) with this setup was 2.003 55, indicating that systematic errors due to field offset were absent.

The one-axis goniometer allowed rotation of the sample around the normal to the horizontal plane containing $\mathbf{B}_0$, and, moreover, the goniometer-cavity assembly could be tilted several degrees in the vertical plane containing $\mathbf{B}_0$. With this facility we could make $\mathbf{B}_0$ follow the (110) plane of the sample to within 0.3° by adjusting the tilt angle to obtain a complete coalescence of corresponding EPR lines from defect sites interrelated through reflection in that plane. The orientation of $\mathbf{B}_0$ within the (110) plane, specified by the angle φ between $\mathbf{B}_0$ and the [001] axis, was determined similarly from the coalescence of symmetry-related lines observed for $\mathbf{B}_0$ directed along the three major axes [001], [111], and [110]. The accuracy achieved was $\pm0.2°$.

The signals $S1_a$ and $S1_b$ discussed here have very similar, near-trigonal g tensors and therefore overlap heavily. Attempts to enhance the separation of the signals by recording the EPR spectra at Q band (35 GHz) rather than at X band were frustrated by a substantial increase of the linewidth: the observed peak-to-peak width of the $S1$ lines was 2–3 times larger at Q band than at X band, suggesting a significant local variation of the g values. Consequently, the small proton hyperfine splitting of the $S1_a$ signal, as well as all but the largest ^{29}Si hyperfine splittings, could only be resolved at X band. The present results are therefore based on X-band spectra in which the desired resolution enhancement was obtained by third-harmonic detection:[23,24] the magnetic field was modulated at 33 kHz, while the EPR signal was lock-in detected at 100 kHz. The signal obtained in this way resembles closely the third derivative of the absorption curve. The peak-to-peak width is reduced compared with that of the first-derivative curve by 26% for Gaussian line shape and 44% for a Lorentzian line shape, and, furthermore, the ''tails'' of the curve are strongly suppressed. As the third-derivative signal is inversely proportional to the fourth

power of the linewidth, detection of relatively weak, narrow EPR lines is possible even when they are almost obliterated by intense, broad lines in the first-derivative spectrum. The third derivative of a Gaussian or Lorentzian line shape has a pair of weak ''sidebands'' on either side of the main peak. These artifacts can be removed by addition of a small-amplitude 100-kHz field modulation to the 33-kHz modulation. In the present experiments no such sidebands were observed, however, so that no 100-kHz modulation was employed. The line shapes of $S1_a$ and $S1_b$ are neither Gaussian nor Lorentzian, which may suggest a superposition of lines with different widths and, hence, account for the absence of sidebands in the resolution-enhanced signals.

C. Derivation of hyperfine parameters

The hyperfine tensors describing ^{29}Si splittings and the proton splitting of $S1_a$ were derived by simulation of the entire spectrum: The spin Hamiltonian term in question was first fitted to the spectra measured with $\mathbf{B}_o$ along [001], [111], and [110]. Subsequently, the results were checked against several spectra having general orientations of $\mathbf{B}_o$ in the (110) plane. Gaussian first-derivative line shapes were used in all simulations. This accounts for some of the residual discrepancies between the simulated and resolution-enhanced experimental spectra. Because the proton hyperfine coupling of $S1_a$ is much smaller than the nuclear Zeeman energy of the proton in the employed field, the proton splitting observed *between* the principal directions strongly reflects the relative signs of the principal values of the hyperfine tensor. This allowed an unambiguous determination of these signs by means of the simulations.

D. Annealing study

A proton-implanted sample was cut in two pieces, which were used for monitoring EPR signals and Si-H stretch modes (by FTIR) after each step in a sequence of 60-min heat treatments in the temperature range 421–674 K. The temperature increment was ~15 K per step. The sample used for EPR was annealed in the microwave cavity with the device described above, whereas the sample used for FTIR was annealed in a furnace in ambient air. The temperature was monitored with identical thermocouples in the two sets of heat treatments. The EPR spectra were recorded at 125 and 312 K, whereas the FTIR spectra were recorded at 12 K.

The Si-H stretch modes, occurring in the spectral range 1800–2250 cm^{-1}, were measured with a Nicolet, System 800, Fourier-transform spectrometer equipped with a glow-bar source, a Ge:KBr beamsplitter, and a mercury cadmium telluride detector. The sample was mounted in a closed-cycle helium cryostat with CsI windows. The apodized resolution was 0.5 cm^{-1}.

III. RESULTS

A. Major EPR transitions

Since no hyperfine splittings from implanted deuterons were resolved, the EPR spectra of Si:D are somewhat simpler than those of Si:H. Therefore, we first discuss the $S1$ signals arising from Si:D.

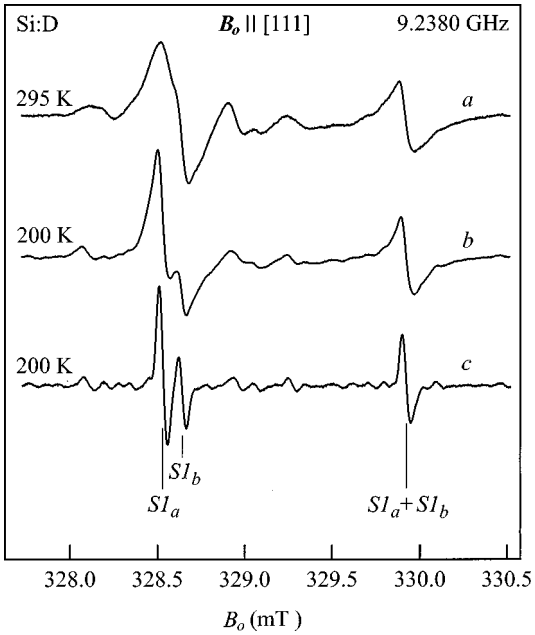

FIG. 1. EPR spectra of deuteron-implanted silicon recorded at two sample temperatures. Curves *a* and *b* are conventional first-derivative spectra, whereas curve *c* was obtained with third-harmonic detection (see text). Main EPR lines belonging to the signals $S1_a$ and $S1_b$ are indicated in curve *c*.

An *X*-band spectrum of Si:D recorded with conventional first-harmonic detection at 295 K with $\mathbf{B}_o$ along the [111] axis is shown in Fig. 1, curve *a*. Two intense lines are observed at 328.6 and 329.9 mT, which agree very well with the positions expected[19–21] for the lines of $S1$. Hence we assign the lines to this group of signals. When the sample temperature is lowered to 200 K, the broad line at 328.6 mT splits into two partially resolved lines[25] (curve *b*). The significant enhancement of the spectral resolution obtained with third-harmonic detection in the present study is demonstrated in curve *c* of the figure.

The $S1$ lines observed at 200 K originate from two distinct, although very similar EPR signals labeled $S1_a$ and $S1_b$ in Fig. 1, curve *c*. When $\mathbf{B}_o$ is along [111], $S1_a$ and $S1_b$ both consist of just two resolved lines, which might seem to indicate that $S1_a$ and $S1_b$ originate from trigonal defects with spin $S=\frac{1}{2}$. However, the spectrum recorded with $\mathbf{B}_o$ parallel to [110] shows that both signals contain four lines for this orientation (Fig. 2), indicating that the symmetry is monoclinic-*I* rather than trigonal.

The monoclinic-*I* symmetry of the $S1_a$ and $S1_b$ defects is confirmed by the variation of the positions of the EPR lines when $\mathbf{B}_o$ is rotated in the (110) plane. Figures 3(a) and 3(b) show the line positions measured at 333 and 200 K, respectively. As described below in Sec. III D, $S1_b$ is observed alone at 333 K. The solid lines in Fig. 3(a) are calculated from the spin Hamiltonian,

$$H=\mu_B \mathbf{S}\cdot\mathbf{g}\cdot\mathbf{B}_0, \tag{1}$$

where μ_B is the Bohr magneton, $\mathbf{S}$ the electron-spin operator ($S=\frac{1}{2}$), and $\mathbf{g}$ a g tensor with monoclinic-*I* symmetry fitted to the data points. The dashed lines in Fig. 3(b) represent the fit to the $S1_a$ data obtained with the spin Hamiltonian of Eq. (1), a monoclinic-*I* g tensor, and spin $S=\frac{1}{2}$. The solid lines

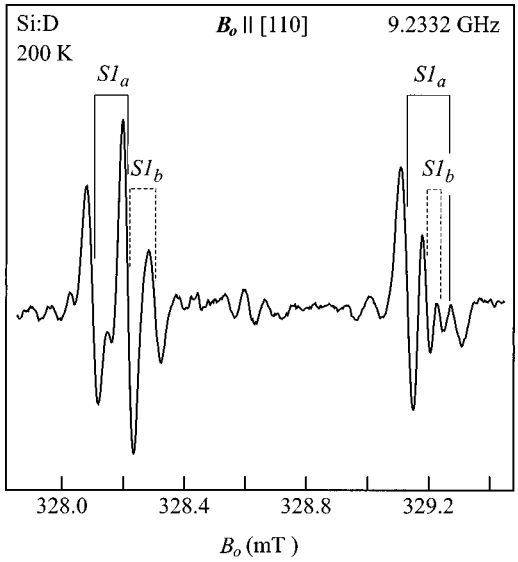

FIG. 2. EPR spectrum of Si:D recorded at 200 K with third-harmonic detection. The main EPR lines belonging to the signals $S1_a$ and $S1_b$ are indicated.

are identical to those in Fig. 3(a). The parameters of the g tensors for $S1_a$ and $S1_b$ are given in Table I together with those obtained previously[16] for $V\mathrm{H}^0$.

B. Hydrogen hyperfine splitting

The spectra of Si:H and Si:D recorded at 150 K with $\mathbf{B}_o$ along [111] and [110] are shown in Fig. 4. The larger number of resolved lines in the Si:H spectra reveals that $S1_a$ exhibits a hyperfine splitting from a single proton. In contrast, no proton hyperfine splitting is resolved in $S1_b$. The $S1_a$ lines in the Si:H spectra were analyzed as described in Sec. II C with the spin Hamiltonian

$$H=\mu_B\mathbf{S}\cdot\mathbf{g}\cdot\mathbf{B}_0+\mathbf{S}\cdot\mathbf{A}_H\cdot\mathbf{I}_H-\mu_N g_H\mathbf{I}_H\cdot\mathbf{B}_0, \qquad (2)$$

where $\mathbf{A}_H$ is the tensor describing hyperfine interaction with the single proton, $\mathbf{I}_H$ is the spin operator for the proton, μ_N the nuclear magneton, and g_H the nuclear g factor for the proton. The components of $\mathbf{A}_H$ obtained from the fit to the $S1_a$ data are given in Table I. It is seen that $\mathbf{A}_H$ is near-axial with the unique axis close to a $\langle 110\rangle$ direction. The stick diagram in Fig. 4 represents the resonant fields of the $S1_a$ and $S1_b$ lines calculated from Eqs. (2) and (1), respectively, with the parameters given in Table I. Simulations of the Si:H spectra, also included in Fig. 4, agree well with the observed spectra. Because the deuteron has nuclear spin $I_D=1$, the $S1_a$ lines in Si:D split into triplets. However, as the nuclear g factor of the deuteron is 6.5 times smaller than that of the proton, the total splitting of a $S1_a$ line is about 3.3 times less in the Si:D spectrum than in the Si:H spectrum, and, hence, remains unresolved.

C. Silicon hyperfine splittings

A wide-range spectrum of Si:D recorded at 150 K with $\mathbf{B}_o$ along [111] is shown in Fig. 5. Each of the strong $S1_a$ and $S1_b$ lines in the central range 327–331 mT has a pair of satellite lines as indicated in the figure. Similar satellites with the same intensity relative to those of the central lines

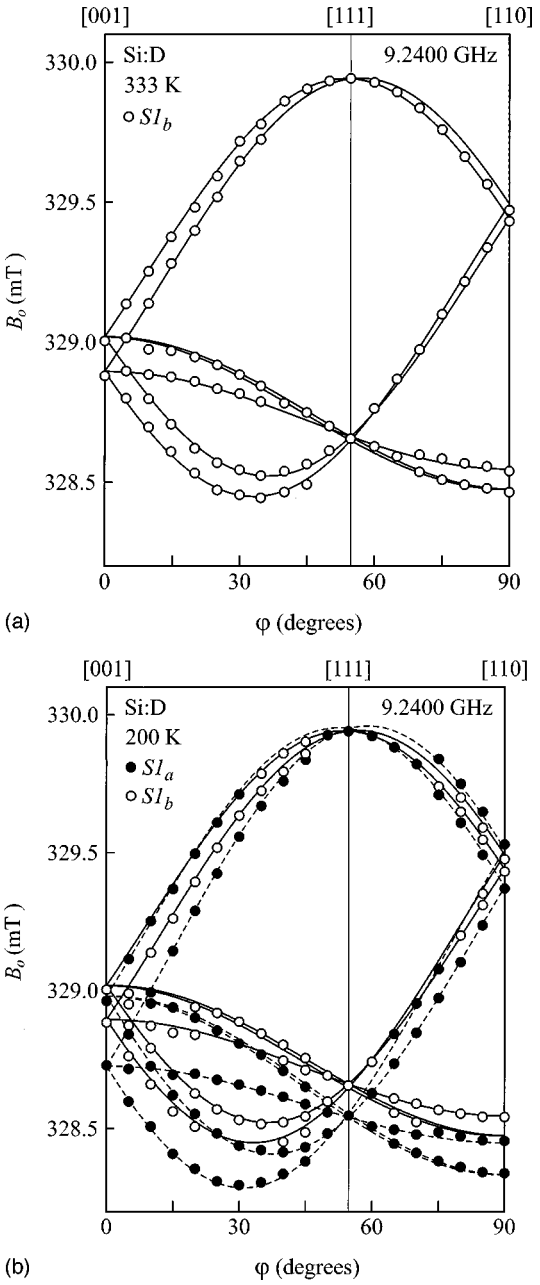

FIG. 3. (a) Angular variation in the $(1\bar{1}0)$ plane of the positions of the EPR lines belonging to $S1_b$. Circles (○) represent the line positions measured at 333 K, and the solid curves show the positions calculated for a defect with $S=\frac{1}{2}$, monoclinic-I symmetry, and the g tensor parameters given for $S1_b$ in Table I. (b) Corresponding angular variations of the $S1_a$ (●) and $S1_b$ (○) signals at 200 K. Dashed curves show the line positions calculated for a monoclinic-I defect with $S=\frac{1}{2}$ and the g tensor parameters listed for $S1_a$ in Table I. The solid lines are identical to those shown in (a).

(~1:40) are observed in the Si:H spectrum. The only silicon isotope with nonzero nuclear spin is ^{29}Si, which has $I=\frac{1}{2}$, and a natural abundance of 4.67%. Therefore, when an unpaired electron interacts with a single silicon atom, the ^{29}Si isotope gives rise to a pair of satellite lines with an intensity ~41 times lower than that of the central line associated with the other isotopes ^{28}Si and ^{30}Si. Accordingly, we assign the satellite lines in Fig. 5 to hyperfine interaction with ^{29}Si located at a unique silicon site.

TABLE I. Spin Hamiltonian parameters for the VH^0 signal, $S1_a$, and $S1_b$. Principal axes are denoted *X*, *Y*, and *Z*, with *Y* parallel to the [110] axis, and *X* and *Z* spanning the (110) plane. Θ is the angle between *Z* and the [110] axis. Principal values of ${}^n\mathbf{A}_{Si}$ and $\mathbf{A}_H$ are given in MHz. Limits of error: **g**, ±0.0001; ${}^n\mathbf{A}_{Si}$, ±1.0 MHz; $\mathbf{A}_H$, ±0.3 MHz.

Term	Principal direction	VH^0	$(S1_a)$ V_2H^0	$(S1_b)$ V_3H^0
g	*X*	2.0090	2.0110	2.0100
	Y	2.0114	2.0100	2.0094
	Z	2.0006	2.0008	2.0009
	Θ	32.4°	31.0°	33.2°
A_H	*X*	−3.3	1.4	
	Y	−4.6	1.6	
	Z	8.5	3.8	
	Θ	8.0°	4.5°	
${}^1\mathbf{A}_{Si}$	*X*, *Y*	−275	−268	−261
	Z	−435	−420	−420
	Θ	35.3°	35.3°	35.3°
${}^2\mathbf{A}_{Si}$	*X*, *Y*	−27	−41	−37
	Z[a]	−34	−48	−43
${}^3\mathbf{A}_{Si}$	*X*, *Y*	−25	−22.5	−23.0
	Z[b]	−40	−36.5	−32.5
${}^4\mathbf{A}_{Si}$	*X*, *Y*	−11		−10.5
	Z[c]	−14		−15.0
${}^5\mathbf{A}_{Si}$	*X*, *Y*	−6		
	Z[c]	−8		
${}^6\mathbf{A}_{Si}$	*X*, *Y*		−10.5	−4
	Z[b]		−13.5	−6

[a]Two equivalent silicon sites. *Z* is taken along $[\bar{1}11]$ and $[1\bar{1}1]$.
[b]Three nearly equivalent silicon sites. *Z* is taken along $[\bar{1}11]$.
[c]Three nearly equivalent silicon sites. *Z* is taken along $[\bar{1}11]$, $[1\bar{1}1]$, and $[11\bar{1}]$.

The ^{29}Si satellite lines have been analyzed with the spin Hamiltonian:

$$H=\mu_B\mathbf{S}\cdot\mathbf{g}\cdot\mathbf{B}_0+\mathbf{S}\cdot{}^1\mathbf{A}_{Si}\cdot{}^1\mathbf{I}_{Si}-\mu_N g_{Si}{}^1\mathbf{I}_{Si}\cdot\mathbf{B}_0, \qquad (3)$$

where ${}^1\mathbf{A}_{Si}$ is the ^{29}Si hyperfine-interaction tensor, ${}^1\mathbf{I}_{Si}$ is the nuclear spin operator, and g_{Si} the nuclear *g* factor for ^{29}Si. Within the limits of error, the ${}^1\mathbf{A}_{Si}$ tensors obtained for $S1_a$ and $S1_b$ are axial with their unique principal axis parallel to the ⟨111⟩ direction along which the unique principal axis (*Z*) of the corresponding *g* tensor is nearly aligned. The principal values of ${}^1\mathbf{A}_{Si}$ are given in Table I.

In addition to the ^{29}Si satellite lines shown in Fig. 5, several pairs of satellite lines with much smaller splittings are observed around the central $S1_a$ and $S1_b$ lines. This is illustrated in Fig. 6, which depicts the spectrum of Si:D recorded at 200 K with $\mathbf{B}_o$ parallel to the [111] axis. The same satellites are observed in the corresponding spectrum of Si:H. Consequently, we assign them to hyperfine interactions with ^{29}Si nuclei. For both $S1_a$ and $S1_b$, two sets of satellites with splittings of the order $\underline{1}$ mT could be resolved for most orientations of $\mathbf{B}_o$ in the (110) plane. One of these sets corresponds to two silicon sites that are equivalent by the mirror symmetry of the defect, and the hyperfine tensors associated with these sites are approximately axial. For the orientation of the defect that has the *Z* axis of the *g* tensor almost aligned with $[1\underline{11}]$, the unique axes of these hyperfine tensors point along [111] and $[1\bar{1}1]$. The other set involves three nearly equivalent silicon sites; the associated hyperfine tensors are

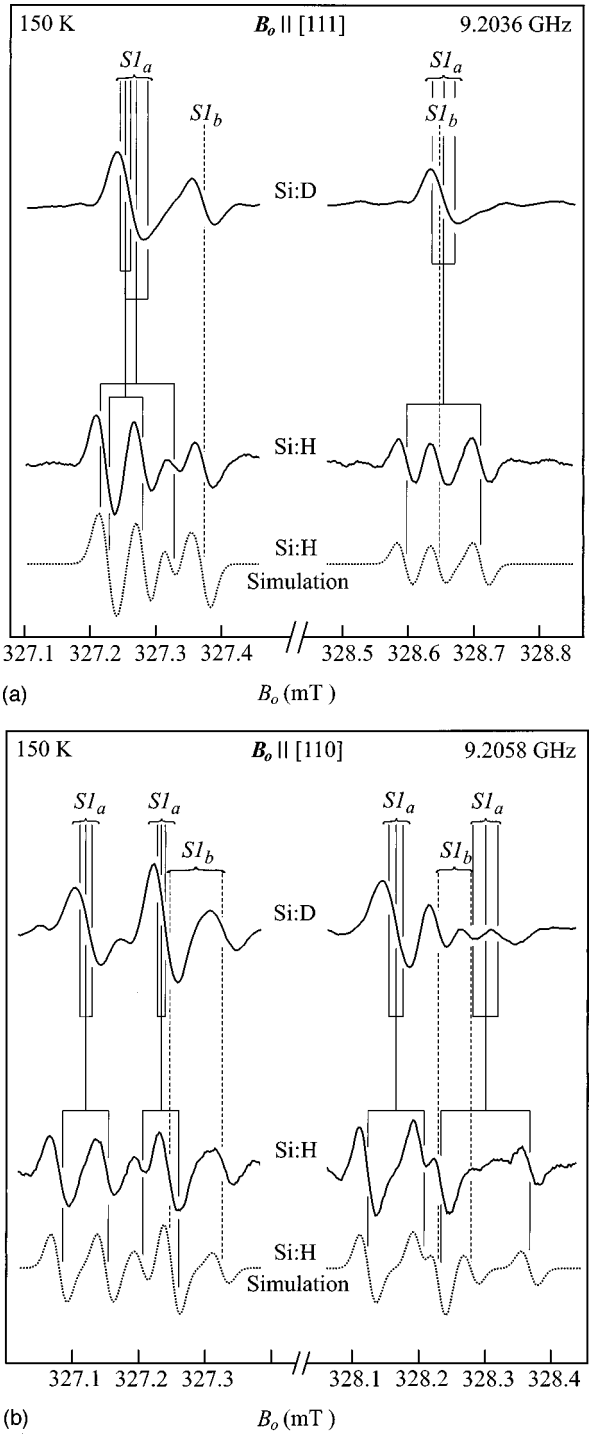

FIG. 4. Comparison of EPR spectra of Si:D and Si:H recorded with third-harmonic detection. Solid curves: observed spectra; broken curves: simulations based on the *g* tensors of $S1_a$ and $S1_b$ and the proton hyperfine tensor A_H for $S1_a$ listed in Table I. The stick diagrams indicate the splitting of the $S1_a$ lines due to hyperfine interaction with the nuclear spins of the deuteron and the proton.

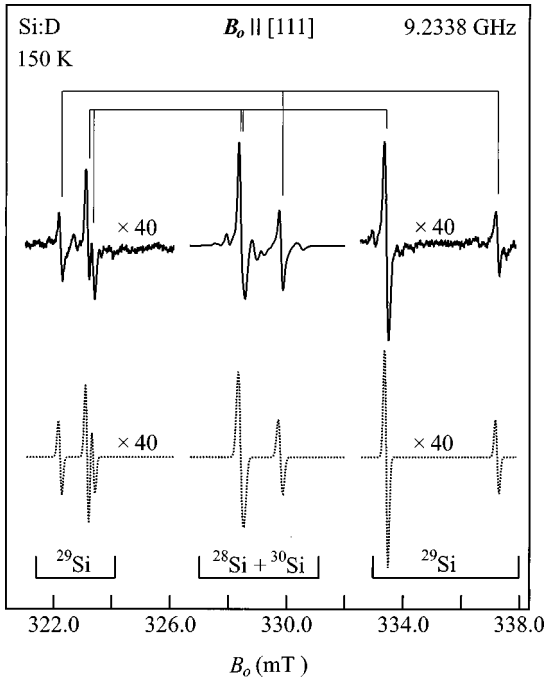

FIG. 5. Wide-scan EPR spectrum of Si:D showing the presence of weak hyperfine satellites to the main lines of $S1_a$ and $S1_b$. Solid curve: observed spectrum recorded at low resolution so that the $S1_a$ and $S1_b$ components of the left-hand main line are barely distinguishable (see Fig. 1, curve *b*). Broken curve: simulation obtained with the trigonal hyperfine tensors $^1A_{\mathrm{Si}}$ listed for $S1_a$ and $S1_b$ in Table I.

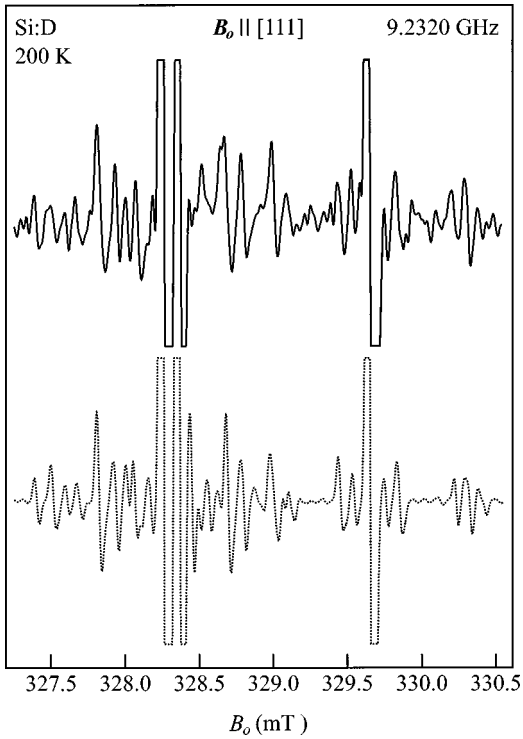

FIG. 6. Central part of the EPR spectrum of Si:D recorded at high gain with third-harmonic detection to show the ^{29}Si-hyperfine structure. Solid curve: observed spectrum; broken curve: simulation obtained with the full set of spin Hamiltonian parameters listed for $S1_a$ and $S1_b$ in Table I.

nearly axial with the unique axes almost parallel to [111]. The available data did not allow a complete determination of the two sets of hyperfine tensors $\{^2\mathbf{A}_{\mathrm{Si}}\}$ and $\{^3\mathbf{A}_{\mathrm{Si}}\}$, describing the satellites. Therefore, the two tensors $\{^2\mathbf{A}_{\mathrm{Si}}\}$, which by symmetry have identical principal values, were taken to be axially symmetric with respect to [111] and [111], whereas three identical axial tensors with axes along [111] were used for the set $\{^3\mathbf{A}_{\mathrm{Si}}\}$. A satisfactory representation of the observed splittings was obtained with the principal values of $^2\mathbf{A}_{\mathrm{Si}}$ and $^3\mathbf{A}_{\mathrm{Si}}$ given in Table I.

Apart from the two sets of ^{29}Si satellites just discussed, $S1_a$ has one additional set and $S1_b$ has two additional sets that are resolved in the spectrum in Fig. 6. It has not been possible to analyze these three sets in detail. Their intensities indicate that they all involve three near-equivalent silicon sites. If it is assumed that each set may be represented by an axial hyperfine tensor with its unique axis along a ⟨111⟩ direction, the principal values and the specific ⟨111⟩ axes may be estimated from the spectrum shown in Fig. 6. The resulting tensors $^4\mathbf{A}_{\mathrm{Si}}$, $^5\mathbf{A}_{\mathrm{Si}}$, and $^6\mathbf{A}_{\mathrm{Si}}$ are included in Table I. A simulation of the Si:D spectrum in Fig. 6 based on the hyperfine tensors described in this subsection is included in the figure. The agreement between the simulated and observed spectrum indicates that the tensors given in Table I account for all prominent ^{29}Si satellites.

In EPR spectra recorded at 45 K, the VH^0 signal displays several sets of ^{29}Si satellites, which are very similar to those observed for $S1_a$ and $S1_b$. The hyperfine tensors deduced from the spectra, which were not reported in Ref. 16, are included for comparison in Table I.

D. Temperature dependence of the *S*1 signals

As noted above, $S1_a$ cannot be observed at sample temperatures $T \geqslant 330$ K. In contrast, $S1_b$ remains observable to 450 K. The gradual, reversible decrease of $S1_a$ with increasing temperature is illustrated in Fig. 7, which shows the high-field part of the Si:H spectrum recorded with $\mathbf{B}_o$ along [111] [see also Fig. 4(a)]. The reduction of the height of the $S1_b$ line roughly reflects the T^{-1} dependence of the difference between the populations of the spin levels involved in the EPR transition. We ascribe the *additional* reduction of the height of the $S1_a$ lines to a thermally induced increase of the linewidth. Since third harmonic detection was employed to resolve the $S1_a$ and $S1_b$ lines in Fig. 7, the signal height (for constant line shape) is inversely proportional to the fourth power of the linewidth, implying that only a minute broadening is required to produce a significant decrease in the observed signal height. Even so, an observable broadening of the $S1_a$ lines should accompany the decay of the signal. However, owing to the strong overlap with the central $S1_b$ line, the broadening of the $S1_a$ lines only emerges when the $S1_a$ and $S1_b$ lines are fitted simultaneously with combinations of Gaussian and Lorentzian line profiles.

E. Thermal decays of EPR signals and Si-H stretch modes

The parallel isochronal annealings of two identical proton-implanted samples, monitored by EPR and FTIR (see Sec. II D), were carried out to search for Si-H stretch modes belonging to VH^0 and to the $S1_a$ and $S1_b$ defects. A section of the FTIR spectrum of Si:H recorded before annealing is shown in Fig. 8. Several sharp absorption lines are observed,

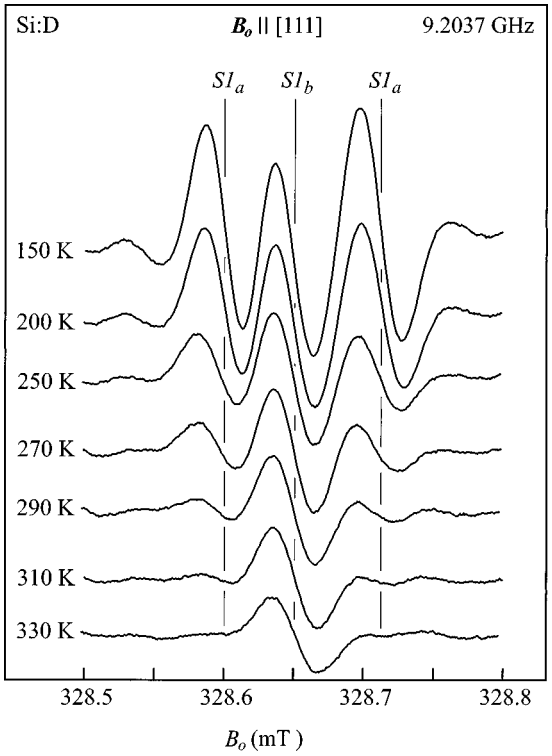

FIG. 7. Temperature dependence of the $S1_a$ and $S1_b$ signals from Si:H, measured with third-harmonic detection. The lines shown are the high-field part of the signals [cf. Fig. 4(a)].

among which those labeled H_2^*, IH_2, and VH_2 were shown previously to represent Si-H stretch modes of these defects.[4–6] The lines at 2038.5, 2068.1, and 2073.2 cm^{-1} all shift downwards in frequency by a factor of $\sim\sqrt{2}$ to 1494.6, 1507.6, and 1511 cm^{-1}, respectively, when hydrogen is replaced by deuterium. Thus these lines also represent local vibrational modes of hydrogen defects and are candidates for Si-H stretch modes associated with VH^0, and the $S1_a$ and $S1_b$ defects.

The spectra recorded during the annealings show that the EPR signal from VH^0 and the mode at 2038.5 cm^{-1} both disappear at about 480 K, whereas $S1_a$ and $S1_b$ and the Si-H modes at 2068.1 and 2073.2 cm^{-1} all decay at about 530 K.

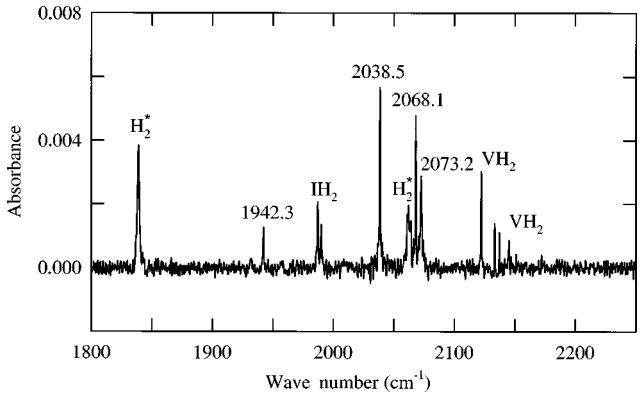

FIG. 8. Section of the FTIR absorbance spectrum of Si:H covering the range of the Si-H stretch modes. The spectrum was recorded at 12 K with an apodized resolution of 0.5 cm^{-1}. Absorption lines previously assigned to specific defect structures are labeled H_2^*, IH_2, and VH_2, respectively.

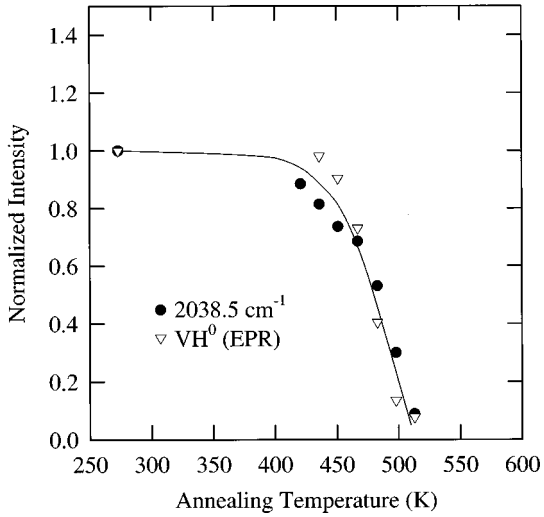

FIG. 9. Thermal decays of the EPR signal from VH^0, and the FTIR line at 2038.5 cm^{-1} as observed in two parts of the same Si:H sample. The intensities of both signals have been normalized to the values obtained after annealing at 273 K.

The thermal decays of VH^0 and of the 2038.5-cm^{-1} mode coincide within the limits of experimental error, as illustrated in Fig. 9. Figure 10 indicates that the same applies to the decays of $S1_a$ and $S1_b$, and of the Si-H modes at 2068.1 and 2073.2 cm^{-1}.[26]

We note that the weak FTIR line at 1942.3 cm^{-1} also decays at about 480 K, and, hence, might seem to be associated with VH^0. However, the initial intensity of this line displays a variation from sample to sample that is unrelated to the variation of the intensity of the VH^0 signal, indicating that the 1942.3-cm^{-1} line originates from a different defect.

IV. DISCUSSION

A. Assignments of $S1_a$ and $S1_b$

The g tensors of $S1_a$ and $S1_b$ and the hyperfine tensors $^1\mathbf{A}_{Si}$ describing the large hyperfine interaction with a ^{29}Si

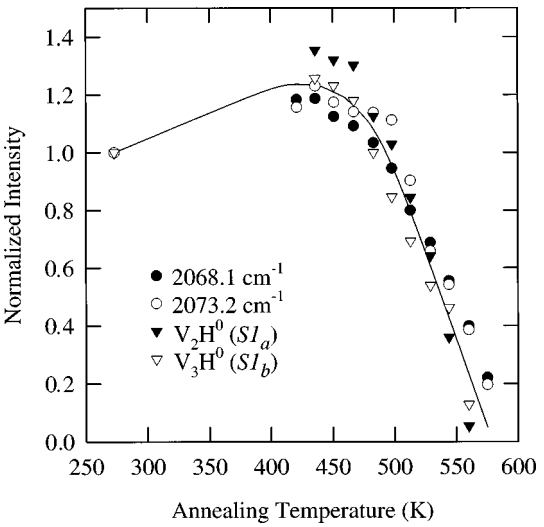

FIG. 10. Thermal decays of the EPR signals $S1_a$ and $S1_b$ and the FTIR lines at 2068.1 and 2073.2 cm^{-1} as observed in two parts of the same Si:H sample. The intensities of both signals have been normalized to the values obtained after annealing at 273 K.

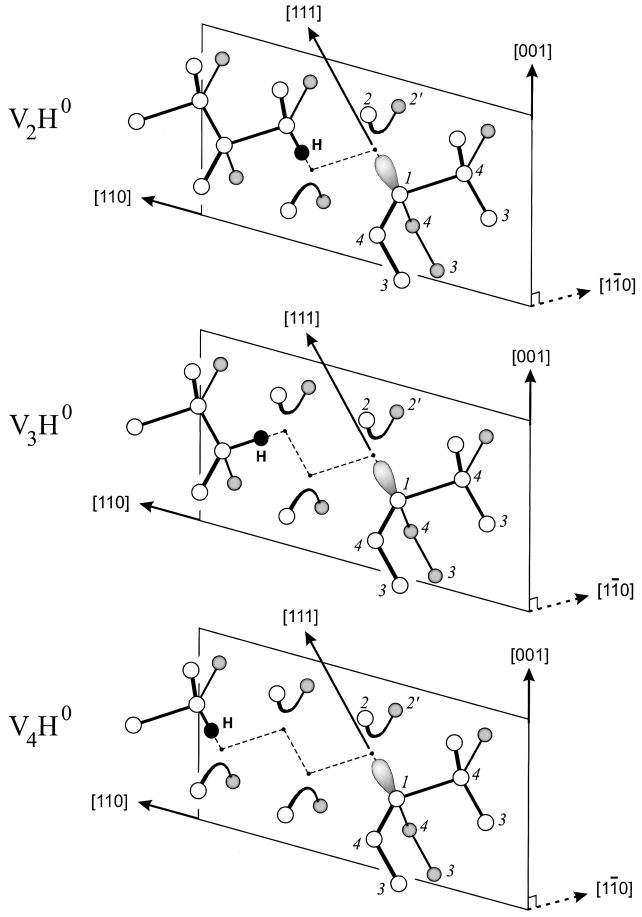

FIG. 11. Sketches of the defects V_2H^0, V_3H^0, and V_4H^0. The silicon sites labeled (1), (2,2′), and (3) give rise to the ^{29}Si hyperfine tensors $^1\boldsymbol{A}_{\mathrm{Si}}$, $^2\boldsymbol{A}_{\mathrm{Si}}$, and $^3\boldsymbol{A}_{\mathrm{Si}}$, respectively.

nucleus at a unique site closely resemble the corresponding tensors determined earlier[16] for $V\mathrm{H}^0$ (Table I). Since $V\mathrm{H}^0$ is a typical vacancy defect in which the unpaired electron resides primarily in a dangling-bond orbital,[27] we therefore assign $S1_a$ and $S1_b$ to vacancy-type defects with a single dangling bond.

The monoclinic-*I* symmetry of the *g* tensors indicates that both defects have a (110) mirror plane. Combined with the presence of a hydrogen atom, established by the hyperfine interaction with a single proton, these observations lead to the identification of the $S1_a$ defect with a member of the family $V_n\mathrm{H}^0$, where V_n denotes a planar cluster of *n* vacancies, forming a zigzag chain in the (110) plane. The unengaged sp^3-like orbitals on the *n* pairs of silicon atoms, bordering V_n symmetrically on either side of the plane, form *n* elongated, weak Si-Si bonds perpendicular to the plane. The corresponding orbitals on the two silicon atoms lying *in* the plane at either end of the vacancy chain interact only weakly, and may in the neutral charge state $V_n{}^0$ of the cluster be considered as dangling bonds. When a hydrogen atom is captured by one of the dangling bonds, a strong Si-H bond is formed, and the electron spin density becomes localized on the other dangling bond at the opposite end of the vacancy chain. The resulting structures of $V_2\mathrm{H}^0$, $V_3\mathrm{H}^0$, and $V_4\mathrm{H}^0$ are sketched in Fig. 11.

The number of vacancies involved in the $S1_a$ defect may be inferred from the observed hyperfine tensor $\mathbf{A}_H$ as follows: The isotropic component $a \equiv \frac{1}{3}(A_X + A_Y + A_Z)$ of the $\mathbf{A}_{\mathrm{H}}$ tensor is 2.3 MHz, which, when compared with the value 1420 MHz characteristic of atomic hydrogen, indicates a near-vanishing electron-spin density at the proton. Therefore, the anisotropic part of $\mathbf{A}_H$ represents a dipolar coupling between the proton spin and the electron spin, which resides predominantly in a ''distant'' dangling-bond orbital. The dipolar hyperfine parameter $b \equiv \frac{1}{6}(2A_Z - A_X - A_Y)$ has the value 0.77 MHz. Within the point-dipole approximation, the distance $\|\mathbf{R}\|$ from the proton to the silicon atom carrying the dangling bond may be estimated by the formula $b = g_e \mu_B g_H \mu_N \|\mathbf{R}\|^{-3}$, where g_e is the *g* factor of the electron. The result is $\|\mathbf{R}\| = 4.7$ Å. Neglecting relaxations around the defect and assuming that the Si-H bond is aligned with a $\langle 111 \rangle$ direction and has the length[15] 1.48 Å, we find that the distance from the proton to the silicon atom carrying the dangling bond is 4.6 Å in $V_2\mathrm{H}^0$, 6.5 Å in $V_3\mathrm{H}^0$, and 8.4 Å in $V_4\mathrm{H}^0$. Consequently, we identify the $S1_a$ defect with $V_2\mathrm{H}^0$. This identification is consistent also with the observed direction of the unique axis *Z* of $\mathbf{A}_H$ which deviates by only 4.5° from the [110] axis: Again neglecting relaxations, we find from the model that the vector connecting the proton and the silicon atom carrying the dangling bond lies 6.3° from the [110] direction.

Apart from the absence of a resolved proton hyperfine interaction, $S1_b$ is very similar to $S1_a$. Moreover, the concentration of $S1_a$ and $S1_b$ defects are equal within a factor of 2, and their annealing behaviors are nearly identical. These findings immediately suggest that the $S1_b$ defect, like the $S1_a$ defect, belong to the $V_n\mathrm{H}^0$ family. Noting also that none of the vacancy clusters V_n identified earlier by EPR (Refs. 17, 18, and 27–29) have spin Hamiltonians consistent with that of $S1_b$, we assign $S1_b$ to $V_3\mathrm{H}^0$. However, we note that the experimental findings do not rule out that larger complexes like $V_4\mathrm{H}^0$ also contribute to $S1_b$. This assignment is consistent with the lack of resolved proton hyperfine splittings of $S1_b$: With the proton-electron separations 6.5 and 8.4 Å estimated from the unrelaxed models of $V_3\mathrm{H}^0$ and $V_4\mathrm{H}^0$ in Fig. 11, the dipolar hyperfine splitting would not be resolved in the EPR spectra. Additional support for the presence of a hydrogen atom in the $S1_b$ defect as well as in the $S1_a$ defect is provided by the observation of Si-H modes with the same annealing behaviors as $S1_a$ and $S1_b$.

B. Interpretation of the small ^{29}Si hyperfine splittings

In addition to the obvious assignment of the large ^{29}Si hyperfine tensor $^1\mathbf{A}_{\mathrm{Si}}$ to the site denoted (1) in Fig. 11, the hyperfine interactions described by the pair of equivalent tensors $\{^2\mathbf{A}_{\mathrm{Si}}\}$ can be associated with the pair of silicon sites labeled (2,2′) in the figure, and with the corresponding sites in $V\mathrm{H}^0$. In the case of $V\mathrm{H}^0$, this follows from the observation of ^{29}Si hyperfine satellites at temperatures where the dangling bond jumps swiftly among the sites 1, 2, and 2′. Under those conditions the satellites correspond to three equivalent silicon sites with unique hyperfine axes along [111], [111], and [111]. Hence these satellites represent the hyperfine interaction averaged over the three equivalent positions of the dangling bond in $V\mathrm{H}^0$. The measured (common) principal values of the hyperfine tensors equal those calculated from the algebraic mean $\frac{1}{3}[^1\mathbf{A}_{\mathrm{Si}}(1) + {}^2\mathbf{A}_{\mathrm{Si}}(2) + {}^2\mathbf{A}_{\mathrm{Si}}(2')]$, which

strongly indicates that the $^2\mathbf{A}_{Si}$ hyperfine tensors represent the spin density at the sites (2) and (2′) when the dangling bond is attached to the site (1).

From the similarity of the tensors $^2\mathbf{A}_{Si}$ of V_2H^0 and V_3H^0 with that of VH^0 (Table I), we infer that $^2A_{Si}$ also for V_2H^0 and V_3H^0 belongs to the pair of equivalent sites (2,2′). We note that Watkins and Corbett[30] earlier carried out a similar analysis of ^{29}Si satellite splittings in the VP^0 signal (*E* center), which closely resembles the VH^0 signal. They obtained the isotropic hyperfine coupling constant $|a|=37.2$ MHz for ^{29}Si located at the pair of sites corresponding to those labeled (2,2′) in Fig. 11. This value of $|a|$ is in fair agreement with the isotropic constants calculated from $^2\mathbf{A}_{Si}$ for all three V_nH^0 defects.

No experimental clue to the origin of the three hyperfine tensors $\{^3\mathbf{A}_{Si}\}$ has been found. It would seem natural to assign them to the three silicon atoms bonded directly to the atom carrying the dangling bond [the sites labeled (4) in Fig. 11]. However, theoretical results for a related defect, the P_b center, indicate that such an assignment is incorrect. The P_b center may be described as a silicon dangling bond at a Si-SiO_2 interface pointing into a microvoid in the silica phase. Accordingly, the essential part of the electronic structure of P_b is expected to resemble a dangling bond in a silicon vacancy. Indeed, the *g* tensor[31] ($g_\parallel=2.0011$, $g_\perp=2.0080$) and the largest ^{29}Si hyperfine interaction[31] ($A_\parallel=-423$ MHz, $A_\perp=-239$ MHz) are similar to those reported here for V_nH^0. The P_b signal furthermore exhibits ''shoulders,'' indicating the presence of additional hyperfine splitting from ^{29}Si described by the hyperfine parameters $A_\parallel=-42.6$ MHz and $A_\perp=-34.9$ MHz, with the unique axis directed within a few degrees along the [111] symmetry axis of the defect. The similarity with $^3\mathbf{A}_{Si}$ of the V_nH^0 defects is evident. Calculations by Cook and White[32] on cluster models of the P_b center unequivocally show that this splitting of the P_b signal originates from a significant spin density on the *second-nearest* neighbors to the atom carrying the dangling bond, corresponding to the sites labeled (3) in Fig. 11. The hyperfine parameters obtained for the relaxed configuration of the model complex $Si_{22}H_{27}$ are $A_\parallel=-36.3$ MHz and $A_\perp=-23.3$ MHz, the unique axis deviating 1.6° from [111], in good agreement not only with the experimental result for the P_b center, but also with the tensors $\{^3\mathbf{A}_{Si}\}$ determined for V_nH^0. In contrast, a near cancellation of direct and polarization contributions to the spin density at the three nearest neighbors [the sites labeled (4) in Fig. 11] reduces the ^{29}Si splittings calculated for these sites to ~6 MHz.[32] On this basis we assign the hyperfine tensors $\{^3\mathbf{A}_{Si}\}$ to the second-nearest neighbor sites (3). Further experiments, e.g., electron nuclear double resonance measurements, are clearly needed before assignments can be made of the weak ^{29}Si hyperfine interactions described by the tensors $^4\mathbf{A}_{Si}$, $^5\mathbf{A}_{Si}$, and $^6\mathbf{A}_{Si}$.

Our assignments imply that only three of the silicon atoms bordering the vacancy chain carry significant electron-spin densities. Moreover, these spin densities are nearly constant through the series VH^0, V_2H^0, and V_3H^0. Hence, not only the *g* tensor but also the detailed distribution of the electron spin is a general characteristic of this kind of defects, and therefore convey little information about the size of the vacancy cluster involved.

C. Motional effects

As noted above, the VH^0 defect reorients[16] when the temperature is raised above ~60 K by bond switching among the three silicon neighbors that do not bind to the hydrogen atom. Unlike VH^0, neither V_2H^0 nor V_3H^0 can reorient into an equivalent configuration solely by a similar rearrangement of the Si-Si bonding. Such a rearrangement would yield a defect with triclinic symmetry, which we suspect will have higher energy than the monoclinic-*I* configuration. This accounts for the absence of motional effects in the temperature range (60–150 K) where the VH^0 signal transforms into a trigonal signal.[16]

Above 200 K, the trigonal VH^0 signal broadens and disappears, possibly due to a rapid motion of the hydrogen atom inside the vacancy. If the hydrogen atom in V_nH^0 similarly jumps among the silicon neighbors above 200 K, a simultaneous reorientation of the dangling bond and the Si-H bond could occur in V_2H^0, implying a rotation of the mirror plane around the ⟨111⟩ axis connecting the two vacancies. A corresponding rotation would not occur in V_3H^0 since this defect is effectively locked to the plane defined by the three vacancies. Therefore, the observation that the $S1_a$ lines broaden and disappear at about 310 K, while the $S1_b$ lines persist to higher temperatures may simply reflect the different geometries of V_2H^0 and V_3H^0.

D. Correlation with Si-H stretch modes

As described in Sec. III E, the VH^0 signal displays the same annealing behavior as the Si-H stretch mode at 2038.5 cm^{-1}, which is one of the most intense modes observed in our samples (see Fig. 8). Furthermore, *in situ* type FTIR studies, which we plan to report in a subsequent publication, have shown that the 2038.5-cm^{-1} mode appears when vacancies become mobile. We conclude that the 2038.5-cm^{-1} mode originates from VH^0.

This assignment is consistent with theory. The Si-H stretching frequencies calculated by several groups[33–35] using different methods are listed in Table II. The frequencies calculated for VH^0 substantially exceed the observed 2038.5 cm^{-1}. This is expected, however, from comparison of the calculated and observed[5,6] frequencies for VH_2 and IH_2. If the ratio between the calculated and observed frequencies is assumed to be roughly the same for different hydrogen defects, the ''true'' frequency of VH^0 may be estimated from those calculated. The results, included as *scaled* frequencies in Table II, range from 2039 to 2119 cm^{-1}. Hence they all deviate by less than 4% from the observed frequency.

As shown in Fig. 10, the thermal decays of $S1_a$ (V_2H^0) and $S1_b$ (V_3H^0) coincide with those of the so far unidentified Si-H stretch modes at 2068.1 and 2073.2 cm^{-1}. Both modes were earlier found to arise from defects containing a single hydrogen atom.[34] In addition, uniaxial stress measurements revealed that the defect giving rise to the mode at 2068.1 cm^{-1} has monoclinic-*I* symmetry, whereas the symmetry of the 2073.2-cm^{-1} defect could not be determined because of overlapping absorption lines.[26,34] On this basis, we ascribe one of these modes to V_2H^0 and the other to V_3H^0. Interpreting the ~30-cm^{-1} increase of the Si-H stretching frequency observed when going from VH^0 to

TABLE II. Comparison of calculated and observed frequencies ω of Si-H stretch modes (in cm^{-1}). ω_B and ω_A denote frequencies of the asymmetric and symmetric stretch modes, respectively. The frequencies in brackets (denoted scaled) are determined from those calculated by multiplication with a common factor that yields the best agreement between the scaled and the observed frequencies for VH_2 and IH_2.

References		VH_2		IH_2		VH^0
		ω_B	ω_A	ω_B	ω_A	ω
Deák *et al.* (Ref. 33)	Calc.			2210	2213	2306
	Scaled			(1987)	(1989)	(2073)
Bech Nielsen *et al.* (Ref. 34)	Calc.	2314	2318	2143	2145	2293
	Scaled	(2138)	(2142)	(1980)	(1982)	(2119)
Park *et al.* (Ref. 35)	Calc.	2268				2168
	Scaled	(2133)				(2039)
This work and Refs. 5 and 6	Obs.	2121.3	2143.8	1986.5	1989.4	2038.5

V_2H^0 (or V_3H^0) as reflecting primarily the reduced interaction between the Si-H group and the dangling bond, we may expect a further, small upwards frequency shift from V_2H^0 to V_3H^0. Hence, we assign the 2068.1-cm^{-1} mode to V_2H^0 and the 2073.2-cm^{-1} mode to V_3H^0. We note that with this assignment, the Si-H stretch frequency of V_nH^0 increases with n and seems to approach the frequency 2086.3 cm^{-1} observed for a Si-H bond on an ideal monohydride (111) surface.[36]

It may be added that Deák *et al.*[33] found that the Si-H stretch frequency of V_2H^+ is 1.1% higher than that of VH^+. If this shift is assumed to apply to V_2H^0 and VH^0 as well, the frequency of V_2H^0 estimated from that of VH^0 is 2061 cm^{-1}—very close to the observed frequency of the mode assigned to V_2H^0.

E. Comparison with earlier work

As mentioned in Sec. I several studies of the $S1$ group of signals have appeared. In the early work,[19–21] these signals were assigned to a single defect with trigonal symmetry. Gorelkinskii and Nevinnyi[12] later found that in proton-implanted float-zone material the $S1$ group consists of two signals which merge to a single signal of trigonal symmetry at high proton doses. No spin Hamiltonian parameters were given for the two signals in Ref. 12, but it is reasonable to assume that these signals are identical to $S1_a$ and $S1_b$.

Dvurechenskii and Karanovich[22] found that the $S1$ defect has monoclinic-I symmetry, and reported g and $^1\mathbf{A}_{Si}$ tensors that are consistent with those of $S1_a$, but they did not observe a second component corresponding to $S1_b$. However, they observed a new signal, labeled $H10$, in phosphorus-rich material irradiated with neutrons. The spin-Hamiltonian parameters of $H10$ are very similar, not only to those of the $B2$ center[37] observed in nitrogen- and phosphorus-implanted material, but also to the parameters of $S1_b$. These surprising similarities may be accounted for in the following way: From our identification of the $S1_a$ and $S1_b$ defects, it may be inferred that the EPR signals from a planar multivacancy with an adjacent substitutional group-V impurity in the mirror plane is virtually indistinguishable from the signal arising from the corresponding defect in which a Si-H unit replaces the group-V impurity. Like the Si-H unit in V_nH^0, the group-V impurity will be located too far from the dangling bond to produce a resolvable hyperfine splitting. Nor can the impurity influence the g tensor significantly. Indeed we were able to resolve a tiny hyperfine splitting from hydrogen in V_2H^0 only because the nuclear g factor of the proton is so large. Thus, the main effect of the group-V impurity or Si-H unit is to dictate an odd number of dangling bonds so that the ground state of the defect has spin $S=\frac{1}{2}$.

Within this framework, the similarity of $B2$ and $H10$ with $S1_b$ may be taken to suggest that $B2$ and $H10$ both belong to a family of defects in which planar vacancies have a group-V impurity atom as a neighbor in the plane. It has often been assumed that the $S1$ and $B2$ defects were identical.[12,20,21] Now, it appears, however, that although their EPR signals are hard to distinguish, these defects belong to two different but closely related families. To reduce the confusion, it might be helpful to reserve the label $S1$ for hydrogen-related defects and use the label $B2$ for the family involving group-V impurities.

Finally, we may comment on the $NL52$ center,[38] which has been observed in proton-implanted float-zone silicon. The principal values of the g tensor of $NL52$ are similar to those of $S1_b$. Moreover, if the weak hyperfine lines ascribed to H_2 in Ref. 38 are instead interpreted as ^{29}Si hyperfine satellites, the principal values of the $^1\mathbf{A}_{Si}$ tensor become $A_Z=-436$ MHz and $A_X=A_Y=-256$ MHz, in good agreement with the parameters found for $S1_a$ and $S1_b$. These observations suggest that the assignment of $NL52$ to H_2 should be reconsidered.

V. SUMMARY

Two EPR signals labeled $S1_a$ and $S1_b$ have been observed in proton-implanted, float-zone silicon. Both signals belong to the $S1$ group and originate from monoclinic-I defects with g tensors that show only a slight deviation from trigonal symmetry. The involvement of a single hydrogen atom in the $S1_a$ defect is proven directly, whereas the evidence of the presence of hydrogen in the $S1_b$ defect is circumstantial. The g tensors and the large ^{29}Si hyperfine splitting associated with a single silicon site correspond to an unpaired electron that occupies a dangling bond in a planar vacancy-type defect binding a hydrogen atom in the plane. From the analysis of the hydrogen hyperfine interaction, the $S1_a$ defect is identified with V_2H^0. The $S1_b$ defect is identified with V_3H^0, although V_4H^0 cannot be ruled out.

In contrast to the VH^0 signal described earlier, $S1_a$ and

$S1_b$ do not display motional effects that may be associated solely with rearrangements of Si-Si bonds. However, $S1_a$ broadens and disappears above 310 K whereas $S1_b$ is little affected. It is suggested that $S1_a$ broadens because the hydrogen atom jumps among the silicon neighbors to the vacancy. In V_2H^0 this may lead to a reorientation of the defect, whereas no reorientation occurs in V_3H^0 since the mirror plane is locked by the three ''immobile'' vacancies.

From parallel annealing studies with EPR and FTIR, it is concluded that VH^0 possesses a Si-H stretch mode at 2038.5 cm^{-1}. In addition, the stretch modes at 2068.1 and 2073.2 cm^{-1} are assigned to V_2H^0 and V_3H^0, respectively.

The EPR spectra of V_nH^0 are similar to that of VH^0, and thus reveal no direct electronic interaction between the Si-H group at one end of the defect and the dangling bond at the other. Hence the length of the vacancy chain could be inferred only in case of V_2H^0 from a tiny dipole-dipole hyperfine interaction with the proton. The number of vacancies separating the Si-H group from the dangling bond *is* reflected, however, in the observed Si-H stretch frequency which increases with increasing chain length.

ACKNOWLEDGMENTS

This work was supported by the Danish National Research Foundation through the Aarhus Center for Atomic Physics (ACAP).

*Author to whom correspondence should be addressed. Electronic address: pj@dfi.aau.dk

[1] See S. J. Pearton, J. W. Corbett, and M. Stavola, *Hydrogen in Crystalline Semiconductors* (Springer-Verlag, Berlin, 1992), and references therein.

[2] See *Hydrogen in Semiconductors*, edited by J. I. Pancove and N. M. Johnson, Semiconductors and Semimetals Vol. 34 (Academic, Boston, 1991), and references therein.

[3] K. Bergman, M. Stavola, S. J. Pearton, and T. Hayes, Phys. Rev. B **38**, 9643 (1988).

[4] J. D. Holbech, B. Bech Nielsen, R. Jones, P. Sitch, and S. Öberg, Phys. Rev. Lett. **71**, 875 (1993).

[5] B. Bech Nielsen, L. Hoffmann, and M. Budde, Mater. Sci. Eng. B **36**, 259 (1996).

[6] M. Budde, B. Bech Nielsen, P. Leary, J. Goss, R. Jones, P. R. Briddon, S. Öberg, and S. J. Breuer, Phys. Rev. B **57**, 4397 (1998).

[7] K. Murakami, N. Fukata, S. Sasaki, K. Ishioka, M. Kitajima, S. Fujimura, J. Kikuchi, and H. Haneda, Phys. Rev. Lett. **77**, 3161 (1996).

[8] A. W. R. Leitch, V. Alex, and J. Weber, in *Defects in Semiconductors 19*, edited by G. Davies and M. H. Nazaré, Materials Science Forum Vols. 258–263 (Trans-Tech, Aedermannsdorf, 1997), p. 241.

[9] A. D. Marwick, G. S. Oehrlein, and N. M. Johnson, Phys. Rev. B **36**, 4539 (1987).

[10] B. Bech Nielsen, J. U. Andersen, and S. J. Pearton, Phys. Rev. Lett. **60**, 321 (1988).

[11] N. M. Johnson, C. Herring, and D. J. Chadi, Phys. Rev. Lett. **56**, 769 (1986).

[12] Yu. V. Gorelkinskii and N. N. Nevinnyi, Physica B **170**, 155 (1991).

[13] B. Holm, K. Bonde Nielsen, and B. Bech Nielsen, Phys. Rev. Lett. **66**, 2360 (1991).

[14] B. Bech Nielsen, K. Bonde Nielsen, and J. R. Byberg, in *Defects in Semiconductors 17*, edited by H. Heinrich and W. Jantsch, Materials Science Forum Vols. 143–147 (Trans-Tech, Aedermannsdorf, 1994), p. 909.

[15] T. L. Cottrell, *The Strengths of Chemical Bonds* (Butterworths, London, 1954), pp. 272–288.

[16] B. Bech Nielsen, P. Johannesen, P. Stallinga, K. Bonde Nielsen, and J. R. Byberg, Phys. Rev. Lett. **79**, 1507 (1997).

[17] J. W. Corbett and G. D. Watkins, Phys. Rev. Lett. **7**, 314 (1961).

[18] Y. H. Lee and J. W. Corbett, Phys. Rev. B **9**, 4351 (1974).

[19] H. Lütgemeier and K. Schnitzke, Phys. Lett. A **25**, 232 (1967).

[20] V. A. Botvin, Yu. V. Gorelkinskii, V. O. Sigle, and M. A. Chubisov, Fiz. Tekh. Poloprovodn. **6**, 1683 (1972) [Sov. Phys. Semicond. **6**, 1453 (1973)].

[21] R. L. Kleinhenz, Y. H. Lee, V. A. Singh, P. M. Mooney, A. Jaworowski, L. M. Roth, J. C. Corelli, and J. W. Corbett, Inst. Phys. Conf. Ser. **46**, 200 (1979).

[22] A. V. Dvurechenskii and A. A. Karanovich, Fiz. Tekh. Poloprovodn. **19**, 1944 (1985) [Sov. Phys. Semicond. **19**, 1198 (1985)].

[23] L. C. Allen, H. M. Gladney, and S. H. Glarum, J. Chem. Phys. **40**, 3135 (1964).

[24] S. H. Glarum, Rev. Sci. Instrum. **36**, 771 (1965).

[25] At sample temperatures below 65 K, a strong EPR signal originating from VH^0 in its stationary form is observed (see Ref. 16) in the field range covered by Fig. 1. Above 125 K, a motionally averaged form of the VH^0 signal appears (see Ref. 16). This motionally averaged signal is visible only in a rather narrow temperature window, and at 200 K it is broadened significantly.

[26] The annealing curve of the 2073.2-cm^{-1} mode is influenced by the overlap with another mode at 2072.4 cm^{-1} that displays a different annealing behavior. Therefore, annealing curves relating to Si-H modes have been determined from the best fit to the absorbance lines obtained with a superposition of Lorentzians with fixed widths.

[27] Y. H. Lee and J. W. Corbett, Phys. Rev. B **8**, 2810 (1973).

[28] G. D. Watkins, J. Phys. Soc. Jpn. **18**, Suppl. II, 22 (1963).

[29] G. D. Watkins, in *Radiation Damage in Semiconductors* (Dunod, Paris, 1964), p. 97.

[30] G. D. Watkins and J. W. Corbett, Phys. Rev. **134**, A1359 (1964).

[31] W. E. Carlos, Appl. Phys. Lett. **50**, 1450 (1987).

[32] M. Cook and C. T. White, Phys. Rev. B **38**, 9674 (1988).

[33] P. Deák, L. C. Snyder, M. Heinrich, C. R. Ortiz, and J. W. Corbett, Physica B **170**, 253 (1991).

[34] B. Bech Nielsen, L. Hoffmann, M. Budde, R. Jones, J. Goss, and S. Öberg, in *Defects in Semiconductors 18*, edited by M. Suezawa and H. Katayama-Yoshida, Materials Science Forum Vols. 196–201 (Trans-Tech, Zürich, 1995), p. 933.

[35] Y. K. Park, S. T. Estreicher, C. W. Myles, and P. A. Fedders, Phys. Rev. B **52**, 1718 (1995).

[36] Y. J. Chabal, Physica B **170**, 447 (1991).

[37] D. F. Daly and K. A. Pickar, Appl. Phys. Lett. **15**, 267 (1969).

[38] P. Stallinga, T. Gregorkiewicz, C. A. J. Ammerlaan, and Yu. V. Gorelkinskii, Phys. Rev. Lett. **71**, 117 (1993).